# THE MAGNET SYSTEM FOR THE BESSY II INJECTOR SYNCHOTRON *

T. Knuth, D. Krämer, E. Weihreter
BESSY II, Rudower Chaussee 5, Geb. 15.1, 12489 Berlin, Germany
I. Chertok, S. Michailov, B. Sukhina
The Budker Institue of Nuclear Physics, SB RAS, Novosibirsk 6300090, Russia

Abstract

Injector for the 3rd generation synchrotron light source BESSY II [1] is a 1.9 GeV full energy 10 cps rapid cycling synchrotron. The 96 m circumference FODO lattice consists of 16 cells having one H-type dipole and the F and D quadrupole magnets on a common girder. A complete pre-series cell has been manufactured by the Budker Institute of Nuclear Physics (BINP), Novosibirsk. Detailed investigations of the field quality were performed at BINP as well as at BESSY.

## I. INTRODUCTION

The lattice structure of the BESSY II booster synchrotron contains 16 bending magnets of 2.62 m length and 32 quadrupole lenses. The energy gain in the booster between injection at 50 MeV and extraction at 1.9 GeV is as large as 38. The dipole field varies according to

$$B(t) = \frac{1}{2} B_\circ (1 - a \cos \omega t) \qquad (1)$$

with $a$ = 0.95, $\omega = 2\pi 10$ cps and $B_\circ = 0.95$ T, thus the resulting field levels are $B_{\rm inj} = 0.025$ T and $B_{\rm ext} = 0.95$ T. The dynamical range for the quadrupole lenses is $g_{\rm inj} = 0.29$ T/m to $g_{\rm ext} = 11.2$ T/m.

BINP manufactured a complete booster cell, fig. 1. Field measurements were performed on the prototypes at Novosibirsk and at Berlin.

## II. DESIGN AND MANUFACTURING OF THE SYNCHROTRON MAGNETS

### *A. Synchrotron Dipoles*

The synchrotron bending magnets, fig. 2, are of H-type. The core is built from four individual blocks forming a polygon rather than having a curved core following the radius of curvature of 6.67 m. Low carbon 2% silicon steel grade GOST 2312 of 0.5 mm thickness is used for the laminations. The coercive force of this steel is within the limit of $H_c = (60 \pm 5)$ A/m. The individual blocks are stacked, pressed between epoxy impregnated end packs and finaly welded to four steel bars to achieve a rigid assembly. The stacking factor is 97.5%. A Rogowski type of chamfer is applied to the ends of the core. The achieved flatness of the poles is 0.08 mm while the gap varied less than $\pm 0.03$ mm for the prototype. The coils are made from rectangular OFHC copper conductor, $22 \times 22$ mm$^2$ in size with a 8 mm diameter cooling duct. Though the large size of the conductor gives eddy current losses of about 0.5 kW in the coil, the total voltage across the dipole circuit does not exceed 3 kV due to the small inductance. Table 1 gives a list of electrical and magnetic data for the bending magnets.

*Funded by the Bundesministerium für Bildung, Wissenschaft, Forschung und Technologie and by the Land Berlin

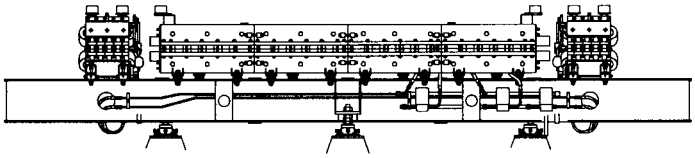

Figure. 1. Unit cell (1/16 of the synchrotron) with one dipole and two quadrupole magnets on a common girder.

| | |
|---|---|
| Magnet | H-type, parallel ends |
| Repetition frequency | 10 cps |
| Max. field | 1 T |
| Gap | 36 mm |
| Core length | 2602.5 mm |
| No of turns | 12 |
| Resistance | 2.87 mΩ |
| Inductance | 2.57 mH |
| Current | 2400 A |
| Power loss | 7.1 kW |

Table I

### *B. Synchrotron Quadrupoles*

For the quadrupoles, the same steel quality and techniques are used as for the dipole. F and D quads are identical, both having a 300 mm long symmetrical core and an aperture radius of $r = 35$ mm, fig. 3. The race track coils are wound from a $12.5 \times 12.5$ mm$^2$ hollow copper profile giving a total voltage drop for each family of 650 V. The main magnetic and electrical parameters are summarized in table 2.

## III. Field Mesurements

Magnetic measurements were performed on the dipole and the quadrupole lenses at BINP using a hall probe array of 11 probes calibrated with NMR. Complete field maps of the dipoles and quadrupoles were measured with the array on a chariot passing on the magnet mid planes. For the harmonic analysis rotating coils were used, and flat coils for AC excitation of the bending magnet. AC measurements of the dipoles and harmonic analysis of quadrupoles were repeated after delivery of the magnets using a DANFYSIK Model 692 harmonic measurement system. Excellent agreement of the measurement results was achieved de-

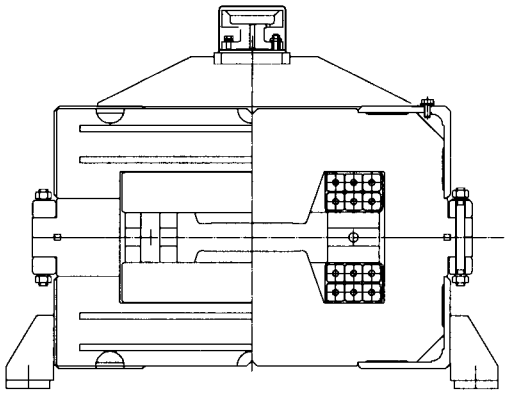

Figure. 2. The synchrotron bending magnet

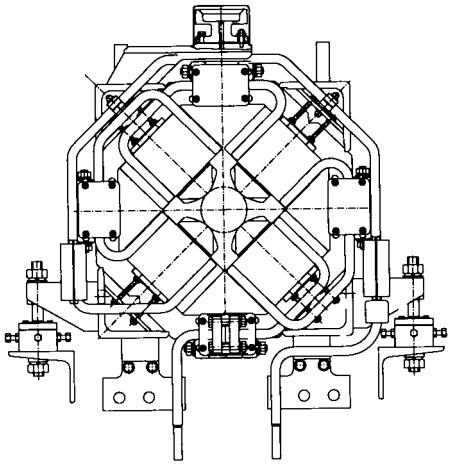

Figure. 3. The synchrotron quadrupole magnet.

spite the 6000 km trip of the synchrotron magnets from the BINP works to Berlin.

### *A. Dipole Field Quality*

The bending strength $\int B \cdot dl$ was determined as a function of the horizontal position at current settings from 60 A to 3000 A, corresponding to fields ranging from 0.025 to 1.25 T, fig. 4. Except for the lowest excitation level, the relative bending strength is constant within $\pm 3.5 \cdot 10^{-4}$ in the good field area of $52 \times 28$ mm$^2$. Only at 250 G the influence of the 11 G remanent field leads to a nonhomogeneity of $\pm 6 \cdot 10^{-4}$.

Electrons were tracked through the mapped DC fields, assuming that the particle momentum corresponds to an exact 22.5° bend. The deviation of the trajectories from the ideally constant radius of curvature was calculated, fig. 5. A maximum deviation of 0.5 mm results from the effective magnetic length which is 11 mm more than the design value of 2619 mm. Therefore, the series magnets will be shortened by this amount, reducing the sagitta to less than 0.1 mm. The offset of the orbit at the magnet exit is due to asymmetries of the field distribution along the beam orbit, leading to amplitudes of 0.2 mm. Again, the remanent field leads to twice this distortion at injection.

| | |
|---|---|
| Magnet type | symmetrical quad |
| Repetition frequency | 10 cps |
| Max. gradient | 14 T/m |
| Aperture radius | 35 mm |
| Core length | 300 mm |
| No of turns | 11 |
| Resistance | 7 mΩ |
| Inductance | 1.76 mH |
| Current | 630 A |
| Power loss | 1.1 kW |

Table II

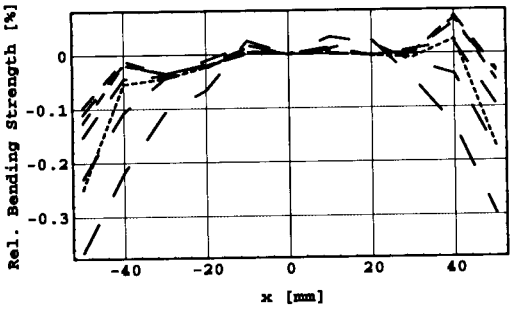


Figure. 4. Relative bending strength in the mid plane for 7 different current settings corresponding to bending fields of 0.025 to 1.25 T.

Measurements at 10 cps AC showed a reduction of the effective magnetic length of up to $7 \cdot 10^{-4}$ during ramping. This effect is due to the eddy current field in the coil overhang. Using the POISSON code [2] the eddy currents were determinded from the field at the location of the individual coil conductors. Thus, the eddy current induced magnetic field was calculated resulting in a time-dependent variation of the bending strength which is shown as a solid line in fig. 6. The agreement with the experimental data is excellent demonstrating that there are no saturation effects at the magnet ends.

### *B. Synchrotron Quadrupole*

A harmonic analysis of the quadrupole lenses was performed at DC for various excitation levels. A typical example for the consistancy of data taken at BINP and by BESSY is shown in fig. 7, where the relative integrated quadrupole strength $d(GL)/GL$ is plotted. The error bars were estimated from a detailed study of the 256 measured angular steps and the fitted harmonics allowing to determine the variance of the multipole coefficients.

The relative gradient distribution $dG/G$ measured with a short coil at the center of the magnet is constant in the mid plane within $\pm 6 \cdot 10^{-4}$.

The integrated quadrupole strength $d(GL)/GL$, fig. 7, shows nevertheless significant contributions of multipoles N = 6 and N = 10 from the fringe field, resulting in non-homogeneity of $d(GL)/GL$ of up to 1.5% in the mid plane. A special chamfer was developped by cutting the outer edges of the poles sensitive

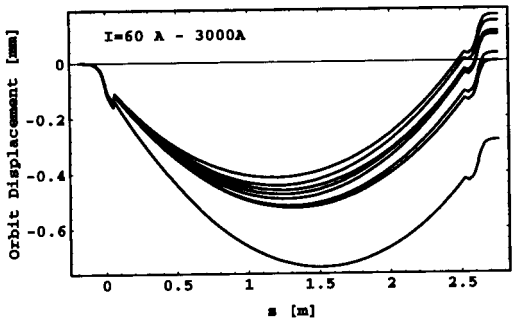


Figure. 5. Difference orbits of tracked particles with respect to an ideal hard edge field distribution for 7 different measured field maps ranging from injection energy to the final energy.

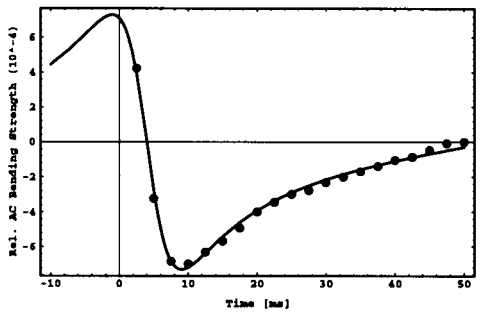


Figure. 6. Calculation of the relative variation of bending strength during the ramp resulting from eddy current fields in the coil (solid curve) compared to experimental data.

to the N = 6 only. By varying the length $L$ of this chamfer the radial homogeneity in the mid plane was considerably improved, fig. 8. At a chamfer length of $L = 31$ mm the dodecapole vanishes completely.

An iso-error curve at $d(GL)/GL < 3 \cdot 10^{-3}$ for the $L = 0$ and $L = 31$ mm chamfer length, fig. 9, demonstrates the significant increase of the physical good field area to 54 mm horizontally and 40 mm vertically for the chamfered magnet. The pattern of the contour clearly resembles the dominating contribution of the N = 6 for no chamfer and N = 10 for the 31 mm deep cut.

## Acknowledgement

The authors would like to thank all staff members of the BINP workshop for the skillful work and their enthusiasm in arranging the prototypes in a time of just 6 month and supplying excellent magnets to the BESSY II project.

## References

[1] E. Jaeschke for the BESSY II team, this conference
[2] Los Alamos Accelerator Code Group, LA-UR-87-115, LANL 1987

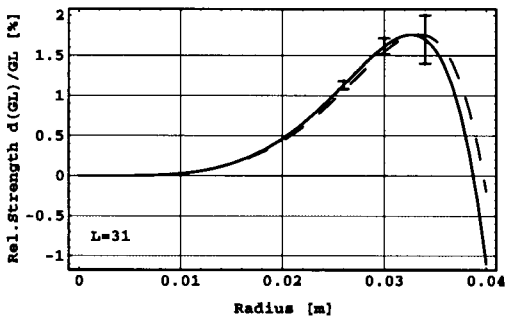


Figure. 7. Relative focussing strength in the mid plane. Dashed curve BINP data, solid curve measurements performed after delivery at BESSY.

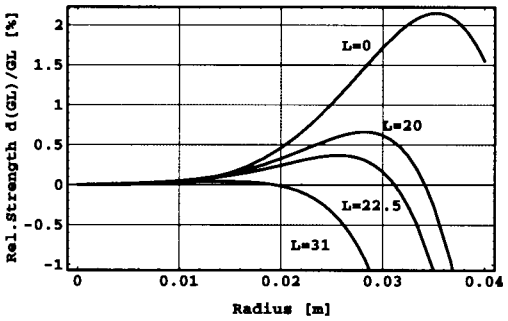


Figure. 8. Relative gradient distributions at mid plane for different chamfer lengths.

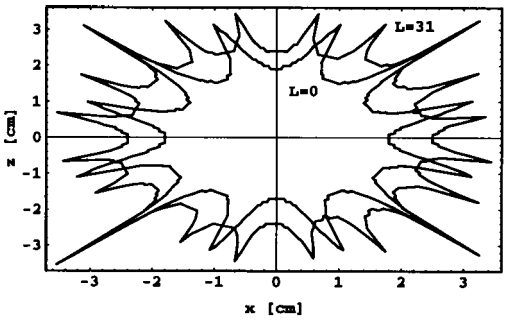


Figure. 9. Iso-error curves for chamfer of $L = 0$ and $L = 31$ mm.